Nano Energy 93 (2022) 106803

Contents lists available at ScienceDirect

Nano Energy

journal homepage: www.elsevier.com/locate/nanoen

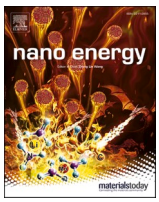

Full paper

Anchoring Interfacial Nickel Cations by Tunable Coordinative Structure for Highly Stabilized Nickel-Rich Layered Oxide Cathodes

Cheng Ma [a,1], Minjian Chen [a,1], Zhengping Ding [b,c,d,1], Bo Wei [e], Chaoping Liang [a], Liangjun Zhou [a], Libao Chen [a], Xiaobo Ji [a,f], Peng Gao [b,c,g], Weifeng Wei [a,*]

[a] State Key Laboratory of Powder Metallurgy, Central South University, Changsha, Hunan 410083, China
[b] International Center for Quantum Materials, and Electron Microscopy Laboratory, School of Physics, Peking University, Beijing 100871, China
[c] Collaborative Innovation Center of Quantum Matter, Beijing 100871, China
[d] School of Materials Science and Engineering, Changzhou University, Changzhou 213164, China
[e] School of Materials Science and Engineering, Beihang University, Beijing 100191, China
[f] College of Chemistry and Chemical Engineering, Central South University, Changsha, Hunan 410083, China
[g] Interdisciplinary Institute of Light-Element Quantum Materials and Research Center for Light-Element Advanced Materials, Peking University, Beijing, China

ARTICLE INFO

Keywords:
Nickel-rich layered oxide cathodes
Highly reactive Ni^{4+} cations
Electron-donating organic groups
Surface coordinative structure
Interfacial stability

ABSTRACT

Ni-rich $LiNi_xCo_yMn_{1-x-y}O_2$ (NCM) cathode materials have received extensive attention on account of their high specific capacities and great application prospects in electric vehicles. While increasing Ni content in NCM can greatly increase initial discharge capacities, more highly reactive Ni^{4+} species in the delithiated state may facilitate irreversible phase transformation and undesirable interfacial reactions, leading to severe capacity degradation. Here we demonstrate an organic surface modification approach to modulate the surface coordinative structure of NCM cathode for enhanced cycling stability. We discover that the highly reactive Ni^{4+} cations can be anchored by strong electron-donating organic groups, especially under bidentate coordination, which mitigates excessive electrolyte decomposition and Ni dissolution into the electrolyte, inhibits the layered-to-rock salt phase transformation and suppresses the initiation and propagation of microcracks within the NCM cathodes. In consequence, the nickel-rich cathode coated with poly (acetoacetoxyethyl methacrylate) (PAAEM) with multiple ester groups exhibits a remarkable improvement in cycling stability, showing 91.3% retention of the initial capacity after 200 cycles. The present findings demonstrate that regulating surface coordinative structure is an efficient and practical strategy to modify the interfacial reactions for enhanced cyclability in Ni-rich layered oxide cathodes.

1. Introduction

Ni-rich layered cathode $LiNi_xCo_yMn_{1-x-y}O_2$ (NCM, $x \geq 0.5$) have been considered as one of the most effective candidates for high-energy lithium batteries with high specific energy over 300 Wh kg^{-1}, opening up a new application prospect in fast-growing electric vehicles (EVs) [1–3]. The $Ni^{2+}/Ni^{3+}/Ni^{4+}$ redox-active couples offer high capacities, however, the intrinsic chemical and structural instability associated with high Ni content, especially at the highly delithiated state, still pose challenging hurdles on their large-scale implementation prospect: (i) excessive electrolyte oxidation/decomposition derived from high catalytic reactivity of Ni^{4+} cations [4,5]; (ii) severe Ni loss engendered by corrosion and dissolution of Ni cations [6–8]; (iii) migration of Ni^{2+} to the neighboring vacant Li^+ sites with concomitant formation of electrochemically inactive NiO-type rocksalt phase[9–11]. Notably, all these issues are mainly initiated at the interface of cathode particles and stabilizing this interfacial layer during charge-discharge process is highly desirable but challenging[12–14].

Surface modification with electrochemically inactive metal compounds (Al_2O_3, [15,16] ZnO, [17,18] MgO, [19] SiO_2,[20] AlF_3, [21] LiF, [22,23]), Li-reactive compounds (Co_3O_4, [24] $Mn_3(PO_4)_2$, [25] $Ni_3(PO_4)_2$, [26]) and Li^+ conductors (Li_3PO_4, [27,28] $LiBO_2$, [29]) have been widely explored to provide a physical barrier to reduce transition metal (TM) dissolution and to suppress side reactions between NCM and

* Corresponding author.
E-mail address: weifengwei@csu.edu.cn (W. Wei).
[1] These authors contributed equally.

https://doi.org/10.1016/j.nanoen.2021.106803
Received 13 October 2021; Received in revised form 23 November 2021; Accepted 2 December 2021
Available online 6 December 2021

non-aqueous electrolytes. Whereas typical inorganic layers are generally thick, inhomogeneous and imperfect coverage, they exert a limited effect on the improvement of long-term electrochemical performance of the NCM cathodes. More recently, with the aid of atomic layer deposition (ALD), Yan et al. successfully coated Li_3PO_4 nanolayer on both surface of primary and secondary particles of polycrystalline Ni-rich $LiNi_{0.76}Co_{0.10}Mn_{0.14}O_2$ cathode and their modified sample demonstrates a superior capacity retention of 91% after 200 cycles [27]. Unfortunately, this advanced ALD process needs to further address its cost-ineffectiveness for the real-world implementation.

Organic surface modification via solvent-based reaction processes is a facile and economical strategy that allows precursor molecules to evenly penetrate into the NCM particles and form a conformal organic nanolayer on NCM cathode [30]. For instance, electronically or ionically conductive polymers, such as polypyrrole (PPy), [31,32] polyaniline (PANI), [33–35] poly(3,4-ethylenedioxythiophene) (PEDOT)[36,37] and poly (ethylene glycol) (PEG) [38] show promise in impeding the interface side reactions and improve electrochemical kinetics. Nevertheless, these conductive polymer layers are physically absorbed to oxide surface and can hardly stabilize interfacial Ni cations and effectively suppress Ni dissolution. Recently, Han et al. designed an ultrathin poly (methyl methacrylate) (PMMA) surface layer for anchoring the Ni^{2+} via electron transfer between the ester group and interfacial Ni^{2+} species [39]. It is worth noting that, however, the PMMA layer may dissolve or decompose under high temperature and high voltage and the incorporation of polyvinylidene fluoride (PVDF) is therefore necessary. Thus far, its ultimate stabilization of Ni cations during extended cycling has not yet been realized and how the Ni-polymer complexing interaction affects interfacial evolution has not been well elucidated.

In this work, we demonstrated a new organic modification strategy that allows organic precursors with tunable complexing sites to coordinate to surface TM cations, especially Ni, suppressing the irreversible phase transformation and dissolution of TM cations and thus substantially mitigating the capacity loss and voltage decay of Ni-rich cathode materials. Specifically, polymeric nanolayers with different functional groups, including poly (2-Cyanoethyl Acrylate) (PCA) with a single cyano-group and poly (acetoacetoxyethyl methacrylate) (PAAEM) with multiple ester groups, were applied to tailor the $LiNi_{0.6}Co_{0.2}Mn_{0.2}O_2$ cathode surface (Fig. 1). First-principles calculations, in situ X-ray diffraction (XRD) and surface structural analyses reveal that the suppressed capacity/voltage decay arises from the effective reduction of reactivity of Ni^{4+} cations on the cathode surface and the retention of interfacial structure over extended cycling, which is dominated by the variable electron-donating capability of the applied organic functional groups. Our findings suggest that tailoring the surface electronic structure via coordination with organic functional groups provides a robust strategy to address the issues of capacity/voltage decay of transition metal-based layered oxide cathodes.

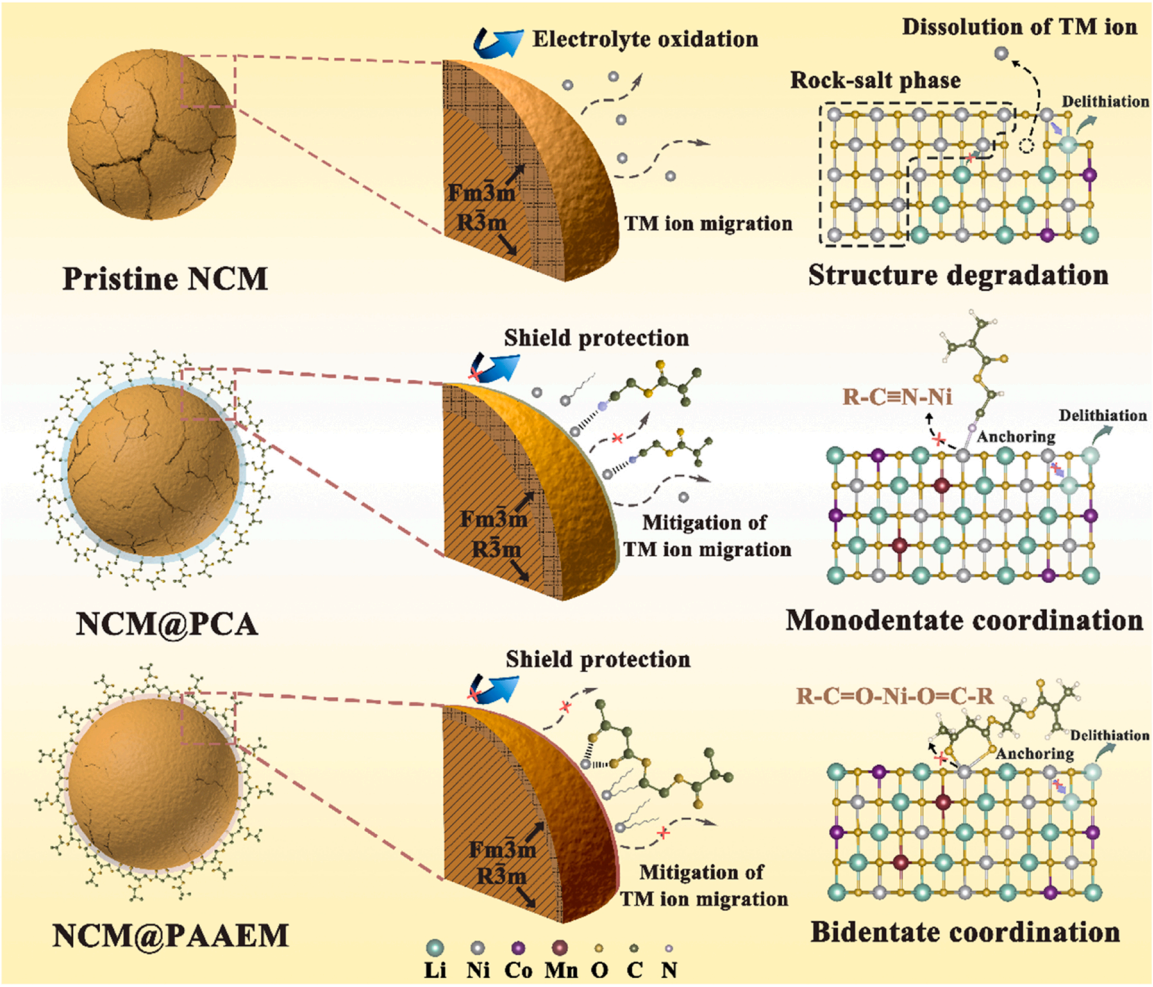

Fig. 1. Schematic diagram for surface coordination mechanism and structural stability differences on NCM cathodes. Severe surface degradation and crack propagation on (a) pristine NCM and improved structural stabilities with relieved particle cracking on (b) NCM@PCA and almost no particle cracking on (c) NCM@PAAEM.

2. Experimental

2.1. Materials synthesis

Ni-rich layered oxide materials were prepared via a co-precipitation and solid-state method [40]. Typically, a transition-metal (TM) solution (2 mol L^{-1}) was prepared by dissolving stoichiometric amounts of $NiSO_4.6\ H_2O$, $CoSO_4.7\ H_2O$ and $MnSO_4{\cdot}H_2O$ in deionized water. The as prepared TM solution, 2 mol L^{-1} of Na_2CO_3 and 0.24 mol L^{-1} of $NH_3{\cdot}H_2O$ were pumped into a 5 L reaction tank with the pH value adjusted to 7.8 and the solution temperature kept at 60 °C. The obtained $(Ni_{0.6}Co_{0.2}Mn_{0.2})CO_3$ precursor was washed by deionized water for several times to remove the residual Na^+ and SO_4^{2-}, and then dried at 100 °C for 24 h. After pretreated at 500 °C for 4 h, the carbonate precursor was mixed with Li_2CO_3 and calcined at 880 °C for 15 h under pure oxygen atmosphere.

The PAAEM and PCA coated $LiNi_{0.6}Mn_{0.2}Co_{0.2}O_2$ particles were synthesized by solution polymerization. Specifically, the acetoacetoxyethyl methacrylate monomers (0.04 g) were dissolved into anhydrous acetonitrile (15 mL), and then the NCM powders (2.0 g) were added. The above-mentioned mixed solution was ultrasonic bathed for 1 h to realize equality dispersion. After adding 2,2'-Azobis(2-methylpropionitrile) into the precursor solution, the monomers were polymerized on the surface of the NCM particles under continuously stirring and heating at 60 ℃ for 4 h in an argon atmosphere. Finally, the NCM@PAAEM powders were collected by rotary evaporation and dried under vacuum at 60 ℃ over 12 h. The NCM@PCA powders were synthesized using the same methods mentioned above.

2.2. Electrochemical measurements

Electrochemical performance measurements were conducted using CR2016 coin type cells with NCM cathode and Li metal anode. To prepare cathode electrodes, a slurry containing the as-prepared samples, carbon black and polyvinylidene difluoride (PVDF) at a weight ratio of 8:1:1 was dispersed in N-methyl-2-pyrrolidone (NMP), and then cast evenly onto an Al foil. After the solvent evaporation under vacuum, the electrodes were punched into wafers with a diameter of 12 mm, and then dried at 110 ℃ for 12 h in a vacuum oven to remove the moisture. The average loading level of cathode active material was about 2 mg cm^{-2}. The cell assembly was executed in an argon-filled glove box ($O_2 < 0.5$ ppm, $H_2O < 0.5$ ppm). The electrolyte was prepared through dissolving 0.6 M lithium bis(trifluoromethanesulphonyl)imide (LiTFSI), 0.4 M lithium bis(oxalato)borate (LiBOB) and 0.05 M lithium Hexafluorophosphate ($LiPF_6$) in the solvent mixture of ethylene carbonate (EC) and ethyl methyl carbonate (EMC) (4:6 by weight). The electrochemical performance of as-assembled cells was evaluated on a LAND-CT2001A battery testing system in a potential range of 3.0–4.3 V (vs. Li^+/Li) at 1C (1C = 160 mAh g^{-1}). Electrochemical impedance spectroscopy (EIS) was performed on a Princeton PARSTAT 4000 using an ac amplitude of 5 mV in a frequency range from 10 mHz to 100 kHz.

2.3. Materials characterizations

The morphology of the as-prepared samples was obtained by scanning electron microscopy (SEM, Nova Nano SEM 230) and transmission electron microscopy (TEM, JEM-2100F). Powder X-ray diffraction (XRD) using a Bruker Advance D8 powder diffractometer was conducted to investigate the crystallographic structure of as-prepared samples. Fourier transform infrared spectroscopy (FTIR, Nicolet 6700) tests were carried out to analyze the surface chemical composition of as-prepared materials. X-ray photoelectron spectroscopy (XPS, ESCALAB 250Xi) was performed to determine the chemical state of the elements and composition of the electrode interface. The binding energies of all XPS spectra were calibrated based on C 1 s peak at 284.8 eV. Inductively coupled plasma-atomic emission spectrometry (ICP-AES) was utilized to analyze the residual concentration of transition metal cations in the organic electrolyte. Before the test, the NCM electrodes, collected from coin cells after 200 electrochemical cycles, were soaked in 2 mL baseline organic electrolytes for 7 days. HAADF imaging and EELS were conducted by using an aberration corrected FEI STEM (Titan Cubed Themis G2) equipped with a 300 kV X-FEG gun to obtain the detailed local structural and chemical information. The beam current was ~50 pA, the convergence semi-angle was 30 mrad, and a collection semi-angle snap was in the range of 80–379 mrad. EELS spectra were acquired on a Gatan Enfinium ER 977 system with a collection semi-angle of 5.9 mrad, convergence semi-angle of 25 mrad, and a dispersion of 0.25 eV/ch. The data was processed by using DigitalMicrograph (Gatan) software. In-situ XRD measurements were performed to investigate the crystallographic structural evolution using an Empyrean 2 X-ray diffractometer with a 2D Vantec detector.

2.4. Calculation methodology

The electron configurations of PAAEM and PCA were calculated by density functional theory (DFT) method using the Gaussian 09 D01 software [41]. The def2-TZVP [42] basis set combined with Lee–Yang–Parr gradient-corrected correlation functional (B3LYP [43]) was applied to the whole calculations. The highest occupied molecular orbital (HOMO) and lowest unoccupied molecular orbital (LUMO) were calculated by Multiwfn 3.7 [44].

First principles calculations were performed using the Vienna ab initio simulation package (VASP) based on DFT with the exchange-correlation functional depicted by the projector augmented wave (PAW) method and the Perdew-Burke-Ernzerhof (PBE) version of the Generalized Gradient Approximation (GGA).

3. Results and discussion

3.1. Theoretical calculations

During the delithiation process, polymer materials could be oxidized by the cathode materials with strong oxidation states. To ensure the high-voltage compatibility of the coating layer, the polymers should have a relatively high electrochemical oxidation potential, which is equivalent to a low highest occupied molecular orbital (HOMO) [45]. The HOMO and lowest unoccupied molecular orbital (LUMO) levels of PAAEM and PCA molecules were calculated by density functional theory (DFT) (Fig. S1). Compared with regular polymer molecules of PEO and PMMA (Fig. 2a), the PAAEM exhibits a relatively lower HOMO, indicative of a higher oxidation resistance than the general ether and ester-based polymers, demonstrating its electrochemical stability against high charge voltage during cycling. As for the PCA, the cyano group can promote electron delocalization of the entire molecule and enhance the oxidation resistance of PCA [46,47]. Additionally, both polar carbonyl and cyano groups can share a pair of electrons with TM cations (Fig. 2b) [48–50]. These results indicated that PAAEM and PCA with high antioxidant ability are suitable coating materials to coordinate the TM cations on the surface of NCM cathode, and thus maintain its structural integrity even after prolonged cycling.

3.2. Structural characterizations

To confirm the polymerization of organic monomers on the surface of NCM particles, Fourier transform infrared (FTIR) spectra of the pristine NCM, NCM@PCA and NCM@PAAEM are compared in Fig. 2c. The FTIR spectra exhibit strong peaks at around 2256, 1726, 1445 and 1155 cm^{-1} that could be assigned to the stretching vibration of C≡N, C═O, C-C and C-O-C, respectively, which are in well accordance with the standard spectra of the PAAEM and PCA monomers, revealing the existence of the polymer layers on the particles (Fig. S2). Scanning electron microscopy (SEM) and transmission electron microscopy (TEM)

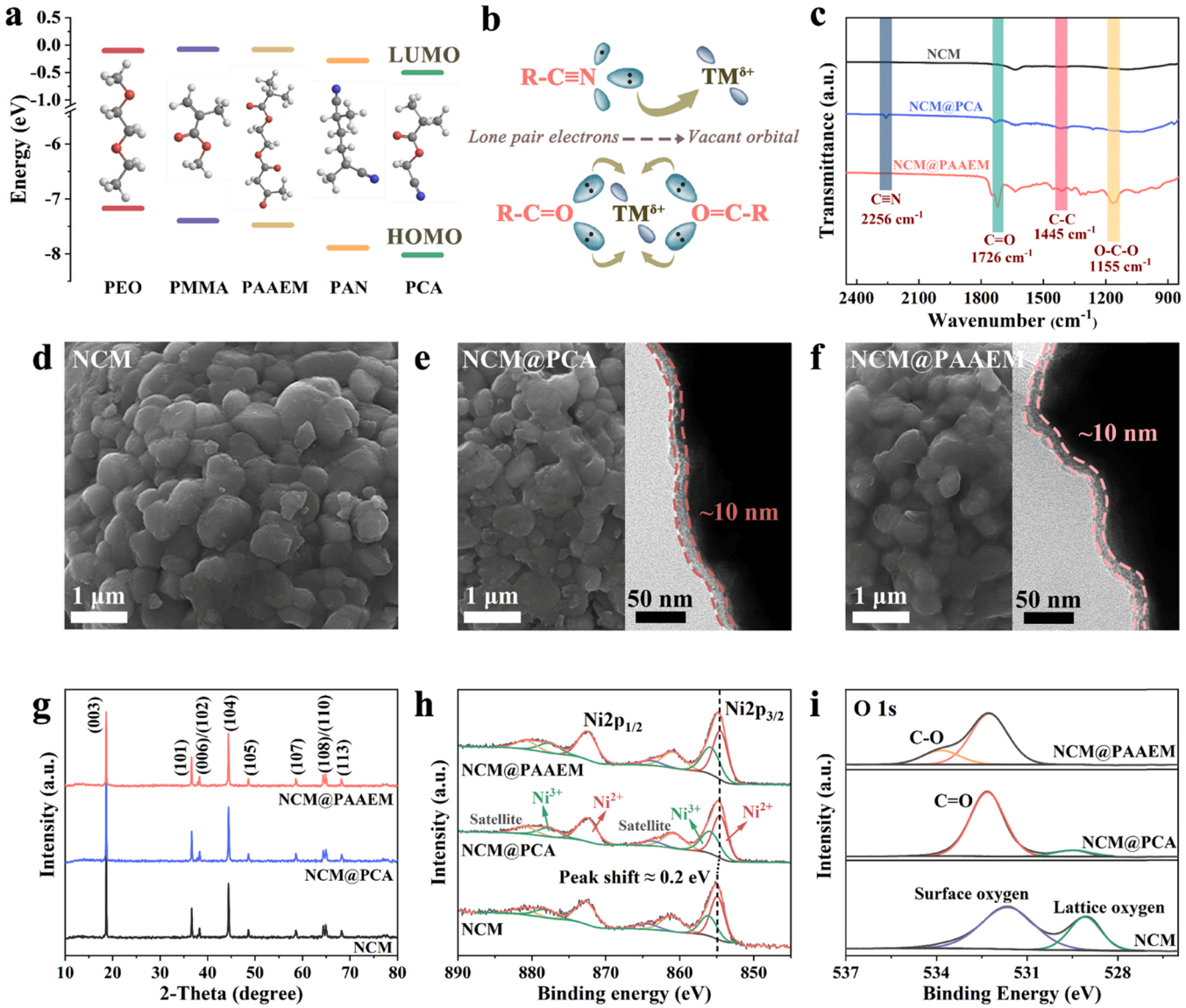

Fig. 2. Theoretical calculations and structural characterizations. (a) Comparison of the highest occupied molecular orbital (HOMO) and lowest unoccupied molecular orbital (LUMO) energy levels for different polymers. (b) The diagram of shared electronic pair between polymer and transition metal ion. (c) FTIR spectra of NCM, NCM@PCA and NCM@PAAEM samples. SEM and TEM images of (d) NCM, (e) NCM@PCA and (f) NCM@PAAEM samples. (g) XRD patterns of NCM, NCM@PCA and NCM@PAAEM samples. XPS spectra for (h) Ni 2p and (i) O 1 s for different samples.

images (Fig. 2d-f and Fig. S3) confirm the polymer nanolayers (~ 10 nm) evenly cover the NCM particles. EDS elemental mappings taken from the cross-sectioned particles (Fig. S4), demonstrate that the polymer nanolayers can penetrate into the NCM particles and thus form a conformal nanolayer. X-ray diffraction (XRD) patterns show no extra diffraction peaks after application of polymer layers compared with the pristine NCM, which suggests the amorphous nature of the coating layers (Fig. 2g and Fig. S5).

In order to investigate the surface coordinative structures, high resolution X-ray photon spectroscopy (XPS) analysis was implemented by using representative Ni 2p and O 1s spectra (Fig. 2h and 2i). The Ni 2p spectra exhibits slight deviation (~ 0.2 eV), shifting to a lower binding energy after polymer coating. This reveals that the introduction of polymer coating layers changes the surface chemical environment of cathode material due to the chemical interaction between organic groups and Ni atoms [51]. Moreover, the surface chemical state of oxygen is likewise altered after coating. The peaks at around 529.1 eV and 531.6 eV represent the lattice oxygen with stable coordination in the bulk and under-coordinated oxygen on the surface, respectively. It is clearly shown that the intensity of both oxygen peaks is attenuated to a marginal level. The emergence of additional peaks at binding energy of 533.8 eV and 532.3 eV, corresponding to C-O and C═O bands, also corroborates that the electronegative polymers PAAEM and PCA were successfully deposited onto the surface of NCM material.

3.3. Electrochemical performance of pristine and polymer-coated NCMs

To evaluate the effect of the applied polymer coatings, the electrochemical performance of pristine NCM and coated NCM was measured (Fig. 3). The NCM@PAAEM and NCM@PCA deliver a slightly lower initial discharge capacity of 178 mAh g^{-1} than the pristine NCM of 182.4 mAh g^{-1} under 0.1C due to the increase of contact resistance between active materials. Nevertheless, as shown in Fig. 3a, the coated samples exhibit higher initial coulombic efficiencies (88.4%, 88.1%) than the pristine NCM (86.5%), indicating effective suppression of irreversible capacity loss. The NCM@PAAEM electrode exhibits remarkable cyclability enhancement with a capacity retention of 91.3% after 200 cycles, when compared with the NCM@PCA and pristine NCM (85.8% and

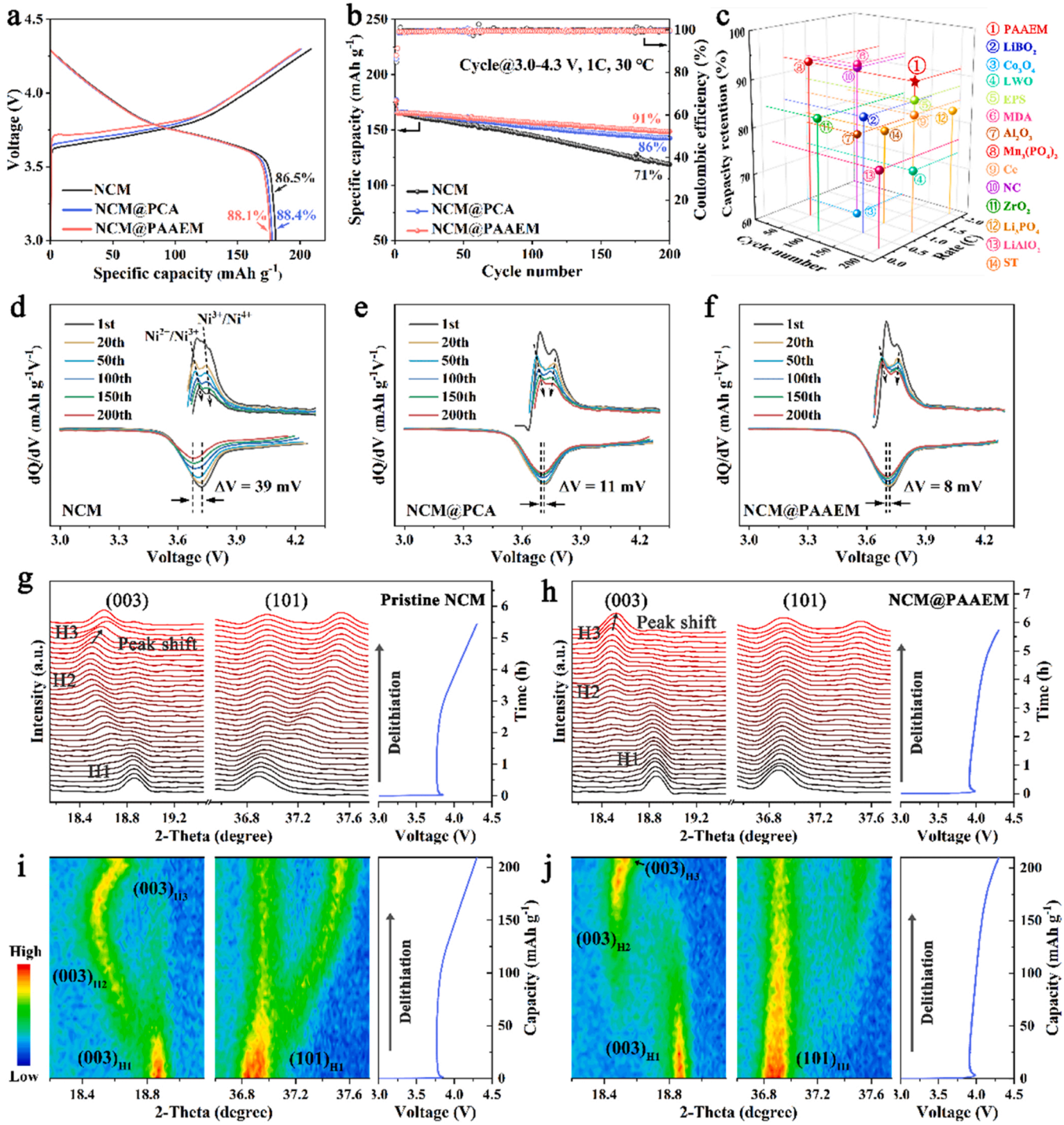

Fig. 3. Electrochemical performance of pristine NCM, NCM@PCA and NCM@PAAEM half cells. (a) Galvanostatic discharge/charge voltage profiles of NCM, NCM@PCA and NCM@PAAEM at 0.1 C. (b) The capacity retention of NCM, NCM@PCA and NCM@PAAEM at 1C. (c) Comparison of the cycling performances of $LiNi_{0.6}Co_{0.2}Mn_{0.2}O_2$ with other reported coating layers (LWO: Li_2WO_4, EPS: ethoxy-functional polysiloxane, MDA: MOF-derived alumina, NC: nitrogen-doped carbon). The dQ/dV profiles of (d) NCM, (e) NCM@PCA and (f) NCM@PAAEM at different electrochemical cycles. In-situ XRD during charging of the pristine NCM in the first cycle, and the corresponding (g) in-situ XRD patterns and (i) contour plots of the (003) and (101) reflections. In-situ XRD during charging of (d) the NCM@PAAEM in the first cycle, and the corresponding (h) in-situ XRD patterns and (j) contour plots of the (003) and (101) reflections.

71.1%, respectively) (Fig. 3b). Note that coated NCM electrodes exhibit optimal cycle stability with the polymer content of 2 wt% (Fig. S6–7), which balances the contact resistance and coordination effect. In addition, the average discharge voltage decreases by 70 mV, 15 mV and 10 mV for the pristine NCM, NCM@PCA and NCM@PAAME after 200 cycles (Fig. S8). The voltage decay trend demonstrates that the polymer layers are beneficial to decrease the electrode polarization, particularly the PAAME layer, which is consistent with the charge/discharge curves in Fig. S9. The cycling performance of NCM@PAAEM excels those of the previously reported NCM622-based cathodes with other inorganic or organic coating materials (Fig. 3c and Table S1), indicating the superiority of the PAAEM coating layer. Additionally, the rate performance of NCM@PCA and NCM@PAAEM is comparable to that of the pristine NCM (Fig. S10).

To precisely probe the polarization evolution upon cycling, differential capacity (dQ/dV) versus voltage curves derived from the charge-discharge profiles are compared in Fig. 3d-f. The gradual peak shift and reduced peak intensity of the redox reactions indicate the accumulation of structure degradation and surface side-reactions of NCM that leads to the increase of capacity fading [52]. In contrast to the remarkable potential deviation (39 mV) and suppressed peak intensity in pristine NCM (Fig. 3d), much less attenuation of the reduction peaks of NCM@PAAEM can be observed after 200 cycles (Fig. 3f). Furthermore, compared with the stable oxidation peaks of the NCM@PAAEM, the Ni^{3+}/Ni^{4+} peak located at around 3.75 V for pristine NCM virtually disappears. This suggests that the strong coordination capability of PAAEM can stabilize the highly reactive Ni^{4+} cations and thus substantially promote the reversibility of the $Ni^{2+/4+}$ redox reactions, which is well consistent with the remarkably decelerated growth of interfacial resistance, as confirmed in the electrochemical impedance spectroscopy (EIS) results (Fig. S11 and Table S2). The positive influence of the coordinative PAAEM layer on the cathode materials is further demonstrated by the improved electrochemical performance of the NCM@PAAEM tested under a higher cut-off voltage of 4.5 V and an elevated temperature of 60 ℃ (Fig. S12–13).

3.4. In-situ XRD analysis

In order to determine the protective behavior of PAAEM polymer coating on the structure of NCM materials, the structural evolution associated with the delithiation process of the pristine and NCM@PAAEM cathodes was investigated using in-situ XRD in a voltage range of 3–4.3 V at a constant current density of 0.2 C. Fig. 3g-j and Fig. S16–17 exhibit the in-situ XRD patterns and contour plots of

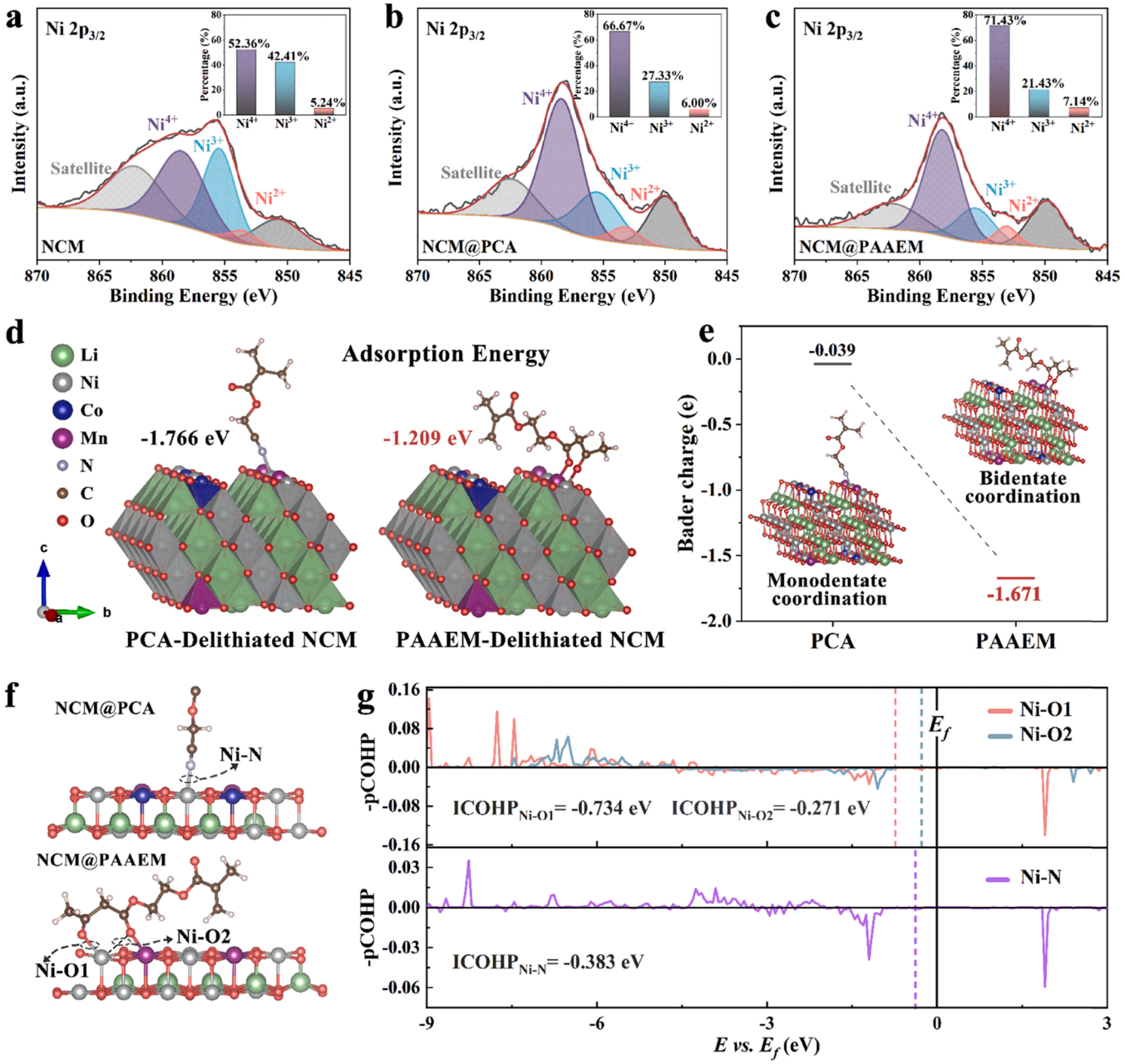

Fig. 4. Coordination mechanisms of PCA and PAAEM coatings on NCM cathodes. Ni $2p_{3/2}$ XPS spectra with fitted components for the (a) NCM, (b) NCM@PCA and (c) NCM@PAAEM samples after initially charged at 4.3 V. (d) The adsorption energy and (e) the balder charge energy for PCA and PAAEM on the delithiated NCM surface. (f) The coordination structure of different polymers and NCM materials. (g) The COHP of Ni-N, Ni-O1 and Ni-O2 coordination bonds.

selected regions during the first charge process, accompanied by the corresponding voltage curves of the batteries with regard to the charging time. It is evident that the peak splitting appears in (003) and (101) reflections when the NCM materials are initially charged above 3.75 V, indicating the formation of H2 phase on the basis of the original H1 phase. And then the (003) reflection shifts to higher 2θ angle after further charging, indicating the formation of H3 phase. Differently, the phase transition processes, especially the transition from H2 to H3, are markedly delayed in the charged NCM@PAAEM cathode. This reveals that the PAAEM coating layer can stabilize the delithiated structure of NCM and is in favor of alleviating the aggravated structural distortion related to H2-H3 phase transition.

3.5. Coordination structural analysis

In order to unravel the stabilizing effect of coating layers, XPS analysis was performed on charged NCM, NCM@PCA and NCM@PAAEM materials (Fig. 4a-c). It has been well recognized that, as charged to the cut-off voltage, Ni^{4+} cations are readily reduced by organic electrolyte and in turn bring about the decrease of the oxidation state of nickel cations [53–55]. This can explain a lower proportion of Ni^{4+} observed in the charged NCM due to the undesirable interfacial reactions occurred (Fig. 4a). Comparatively, the incorporation of polymer coatings, in particular the PAAEM layer, facilitates the cathodes maintaining a relatively larger amount of Ni^{4+} cations, suggesting the effective mitigation of side reactions on the cathode-electrolyte interface. The XPS results also illustrate that the protective effect of the polymer coatings is dependent on the coordination bond strength of the applied functional groups. The two carbonyls in PAAEM unit can coordinate with a Ni cation to form a hexagonal ring configuration, stabilizing Ni cations through chelation effect. By comparison, the monodentate coordination between cyano group and Ni cation shows relatively lower structural stability. Moreover, the XPS results of Co and Mn collected from the batteries charged to 4.3 V, as shown in Fig. S14, illustrate that the coordination interaction has little effect on the oxidation state of Mn and Co cations.

To rationalize this coordination mechanism, the adsorption energy, Bader charge transfer analysis and crystal orbital Hamiltonian population (COHP) were calculated to analyze atomic interactions between polymer molecules and NCM under the delithiated state. The adsorption energy of PCA and PAAEM to the NCM surface are − 1.209 and − 1.766 eV respectively, indicating that the two polymers are easily adsorbed on the NCM surface (Fig. 4d). As predicted, the PAAEM molecule shows a much higher Bader charge energy of − 1.671 eV to Ni atom than that of − 0.039 eV for the PCA molecule (Fig. 4e). These results reveal that both the carbonyl and cyano groups have a high ability to donate electrons to Ni atoms and thus form stable coordination bonds [56]. Compared with the monodentate ligand provided by PCA, PAAEM not only possesses multiple carbonyls groups linked to the backbone, but also exists additional β-keto esters on the flexible branched chain (Fig. 4f), which ensures a higher electron-donating capability of PAAEM than that of PCA. COHP was utilized to further analyze the bonding and antibonding information, and the negative COHP value implies the existence of coordination bonds between organic groups and Ni atoms. The results in Fig. 4g confirms that the two Ni-O (Ni-O_1 and Ni-O_2) bonds induced by PAAEM molecule can form six-membered chelating coordination with Ni cations, whereas only one Ni-N coordination bond exists between PCA molecule and Ni. The COHP integrals of Ni-O_1, Ni-O_2 and Ni-N bonds are − 0.734, − 0.271 and − 0.383 eV, respectively, revealing stronger coordination interactions to immobilize Ni^{4+} in NCM@PAAEM than that in NCM@PCA [57].

3.6. Atomic-scale interfacial characterization of the cycled cathodes

To understand the surface chemical evolution along the cathode-electrolyte interface after extended cycles, O 1s XPS spectra of the cycled cathodes were collected (Fig. S15). Compared with NCM@PCA and NCM@PAAEM, the O 1s spectrum in the pristine NCM shifts to high binding energy with stronger peak intensity of C-O (533.3 eV) and CO_3^{2-} (531.2 eV) derived from the decomposition of electrolyte, indicating that the PCA and PAAEM nanolayers effectively protect cathode materials from electrolyte corrosion. This protective effect is also verified by the corresponding inductively coupled plasma-atomic emission spectrometry (ICP-AES) analysis of the residual TM-cation concentrations in the electrolyte (Fig. S16). Consequently, the polymer coatings could slow down the undesirable side reactions, suppress the dissolution of TM cations from the NCM cathode and then improve the cathode-electrolyte interfacial stability by tunable coordination interactions.

Meanwhile, as depicted in the cross-sectioned SEM images of the cathodes after charged to 4.3 V (Fig. S19), the applied polymer coating layers, especially PAAEM, can substantially retain intergranular cracking in polycrystalline NCM cathodes. Since the initiation and propagation of microcracks have been considered to be closely connected with the lattice mismatch between rock-salt and layered phases [58], high angle annular dark field-scanning transmission electron microscopy (HAADF-STEM) characterization was performed to investigate the microstructure changes in pristine and polymer-coated cathodes after 200 cycles. Evidently, the layered structure of pristine NCM gradually transforms into the electrochemically inactive rock-salt phase from the surface to the bulk (Fig. 5a-c and Fig. S20). In contrast, benefiting from suppressed phase transformation as confirmed by in-situ XRD (Fig. 3g-j), the NCM@PAAEM electrode exhibits noticeable improvement in structural integrity. The thickness of rock-salt phase is remarkably reduced to several nanometers on the outer surface (Fig. 5g-i and Fig. S22), which may account for little intergranular cracking in the NCM@PAAEM cathode. Moreover, the NCM@PCA electrode also shows a certain improvement in structural integrity (Fig. 5d-f and Fig. S21).

Electron energy loss spectroscopy (EELS) line-scanning was conducted to investigate the local chemistry evolution from the surface to the bulk of the cycled NCM and NCM@PAAEM materials (Fig. 5j-k). Compared with the bulk region, the Ni-$L_{2,3}$ peaks of the cycled NCM exhibit slight deviation to a lower energy on the surface, which indicates a lower Ni oxidation state on the surface region [59,60]. By comparison, no detectable shift of the Ni-$L_{2,3}$ peak can be observed on the NCM@PAAEM particle, revealing a stable chemical structure is maintained during the long-term cycling. In addition, the O K-edge prepeak of the cycled NCM weakens as well as shifts to higher energy, indicating that the average valence of TM cations decreases during long-term cycling. In contrast, the cycled NCM@PAAEM exhibits minor peaks shifts and intensity variation. he structural and chemical variations demonstrate that the strong coordination complexation between PAAEM and Ni^{4+} cations could effectively suppress the reduction of reactive Ni^{4+} cations to a lower oxidation state in the delithiated state and thus mitigate the degree of Li/Ni cation mixing, thereby conducing to the outstanding structural stability along with cycling performance of the NCM materials.

4. Conclusion

The coordination structures between electron-donating functional groups and Ni^{4+} cations can lead to more general discussions on the interfacial stability of Ni-based cathode materials upon cycling. As discussed previously, highly reactive Ni^{4+} cations at delithiated state are apt to oxidize the organic electrolyte and result in the decrease of the oxidation state of surface Ni cations, which promote the migration of Ni^{2+} cations to Li layer and facilitate the layered-to-rocksalt (NiO) transformation during the subsequent discharge process (Fig. 5a-c). The higher Ni content in the surface rocksalt (NiO) phase brings about the preferential dissolution of Ni in the electrolyte (Figure S16). The cumulation of these detrimental issues results in the initiation of intergranular crack formation at the cathode-electrolyte interface. Gradually, the propagation of microcracks allow the penetration of organic

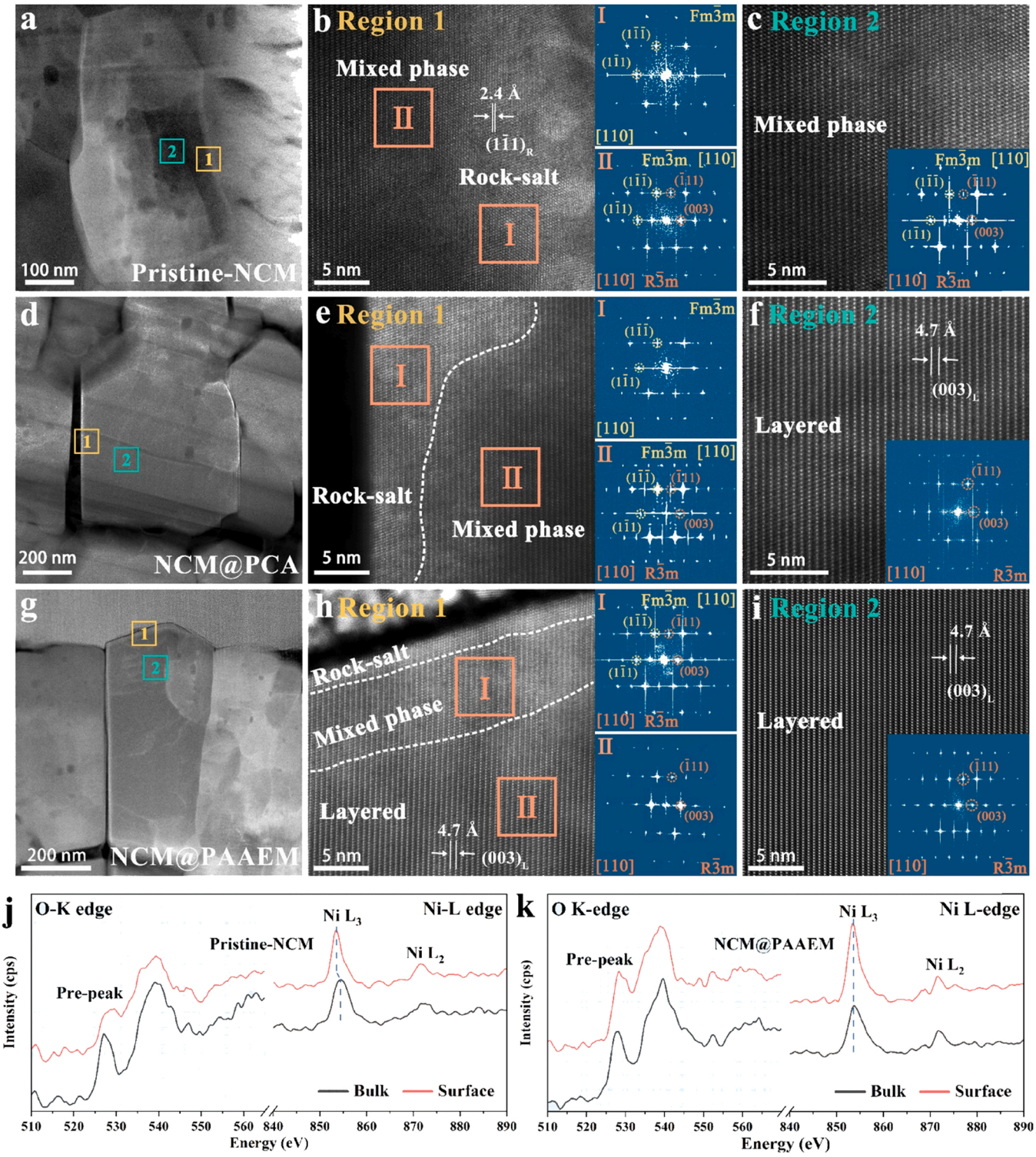

Fig. 5. Structural stability of different samples after cycling. (a) Low-magnification HAADF–STEM image of the pristine NCM after 200 cycles at 3.0 – 4.3 V. (b) Magnified HAADF–STEM image and corresponding FFT patterns taken from region 1. (c) Atomic resolution HAADF–STEM image and corresponding FFT pattern taken from region 2. (d) Low-magnification HAADF–STEM image of the NCM@PCA after 200 cycles at 3.0 – 4.3 V. (e) Magnified HAADF–STEM image and corresponding FFT patterns taken from region 1. (f) Atomic resolution HAADF–STEM image and corresponding FFT pattern taken from region 2. (g) Low-magnification HAADF–STEM image of the NCM@PAAEM after 200 cycles at 3.0 – 4.3 V. (h) Magnified HAADF–STEM image and corresponding FFT patterns taken from region 1. (i) Atomic resolution HAADF–STEM image and corresponding FFT pattern taken from region 2. EELS spectra for the O K-edge and Ni L-edge from the surface to the bulk of the pristine NCM (j) and the NCM@PAAEM (k).

electrolytes into the secondary particles and expose the subsurface of primary particles to the interfacial side reactions, which create a vicious circle for interfacial degradation and cycling instability.

The existence of robust coordination structures induced by the polymeric coatings could bring about multiple benefits as follows. First, strong electron-donating capability of functional groups help stabilizing the high oxidation state of surface Ni^{4+} cations upon charging and refrain Ni cations from migrating to form inactive rocksalt (NiO) phase, both of which substantially promote the reversibility of the Ni^{2+}/Ni^{4+} redox reactions and ensure high reversible capacity of cathodes during extended cycles. Second, the conformal polymeric coatings effectively avoid the direct contact between the organic electrolyte and active NCM cathode materials and thus minimize the excessive electrolyte decomposition and detrimental TM corrosion, leading to less cathode-electrolyte interphase (CEI) and improved interfacial stability. Third, the high flexibility of polymeric coatings may accommodate the repeating volume changes of the NCM particles during charge-discharge process and help mitigate the initiation and propagation of microcracks within the NCM particles.

In summary, we demonstrated an organic surface modification strategy to tune the surface coordinative structure of Ni-rich NCM cathode for enhanced cycling stability by constructing polymeric nanolayers with different functional groups. In situ XRD and surface structural analyses and DFT calculations demonstrated that strong electron-donating capability of functional groups help stabilizing the highly reactive surface Ni^{4+} cations and thus suppress the organic electrolyte decomposition, the layered-to-rocksalt (NiO) transformation and subsequent Ni dissolution in the electrolyte, and the formation and propagation of microcracks within the NCM particles. As a result, $LiNi_{0.6}Co_{0.2}Mn_{0.2}O_2$ cathode coated with PAAEM with multiple ester groups, exhibited a remarkable improvement in cycling stability (91.3% retention rate, 200 cycles). This work provides a new direction to regulate the surface coordinative structures of high capacity and high voltage layered cathode materials for enhanced cyclability.

CRediT authorship contribution statement

Cheng Ma: Conceptualization, Methodology, Validation, Investigation, Writing – original draft. **Minjian Chen:** Methodology, Validation, Investigation, Data curation, Writing – original draft. **Zhengping Ding:** Methodology, Investigation, Writing – review & editing. **Bo Wei:** Theoretical calculation, Validation, Software. **Chaoping Liang:** Software, Validation, Formal analysis. **Liangjun Zhou:** Project administration, Resources, Supervision, Writing – review & editing. **Libao Chen:** Project administration, Resources, Supervision, Writing – review & editing. **Xiaobo Ji:** Project administration, Writing – review & editing. **Peng Gao**: Project administration, Resources, Writing – review & editing. **Weifeng Wei:** Conceptualization, Writing – review & editing, Supervision, Resources, Project administration, Funding acquisition.

Declaration of Competing Interest

The authors declare that they have no known competing financial interests or personal relationships that could have appeared to influence the work reported in this paper.

Acknowledgments

The authors would like to acknowledge financial support from the National Natural Science Foundation of China (51304248, 11874199, 51971250, 52021006 and 11974023), the National Key Research and Development Program of China (Grant No. 2018YFB010400), SAFEA: High-End Foreign Experts Project (Grant No. B06020), the National Basic Research Program of China (Grant No.2015CB654901), the State Key Laboratory of Powder Metallurgy at Central South University and the Shenzhen GuoTuo Technology Co., Ltd.

Appendix A. Supporting information

Supplementary data associated with this article can be found in the online version at doi:10.1016/j.nanoen.2021.106803.

References

[1] Y.K. Sun, S.T. Myung, B.C. Park, J. Prakash, I. Belharouak, K. Amine, Nat. Mater. 8 (2009) 320–324.
[2] V. Etacheri, R. Marom, R. Elazari, G. Salitra, D. Aurbach, Energy Environ. Sci. 4 (2011) 3243–3262.
[3] J.U. Choi, N. Voronina, Y.K. Sun, S.T. Myung, Adv. Energy Mater. 10 (2020) (202002027).
[4] W. Liu, P. Oh, X. Liu, M.J. Lee, W. Cho, S. Chae, Y. Kim, J. Cho, Angew. Chem. Int. Ed. 54 (2015) 4440–4457.
[5] S.H. Lee, J.Y. Hwang, S.J. Park, G.T. Park, Y.K. Sun, Adv. Funct. Mater. 29 (2019), 1902496.
[6] J.R. Croy, D.C. O'Hanlon, S. Sharifi-Asl, M. Murphy, A. Mane, C.-W. Lee, S.E. Trask, R. Shahbazian-Yassar, M. Balasubramanian, Chem. Mater. 31 (2019) 3891–3899.
[7] W. Li, X. Liu, Q. Xie, Y. You, M. Chi, A. Manthiram, Chem. Mater. 32 (2020) 7796–7804.
[8] S. Jurng, S.K. Heiskanen, K.W.D.K. Chandrasiri, M.Y. Abeywardana, B.L. Lucht, J. Electrochem. Soc. 166 (2019) A2721–A2726.
[9] H. Cha, J. Kim, H. Lee, N. Kim, J. Hwang, J. Sung, M. Yoon, K. Kim, J. Cho, Adv. Mater. 32 (2020), 2003040.
[10] S.-K. Jung, H. Gwon, J. Hong, K.-Y. Park, D.-H. Seo, H. Kim, J. Hyun, W. Yang, K. Kang, Adv. Energy Mater. 4 (2014), 1300787.
[11] J. Zheng, Y. Ye, T. Liu, Y. Xiao, C. Wang, F. Wang, F. Pan, Acc. Chem. Res. 52 (2019) 2201–2209.
[12] L. Yang, K. Yang, J. Zheng, K. Xu, K. Amine, F. Pan, Chem. Soc. Rev. 49 (2020) 4667–4680.
[13] S.K. Heiskanen, N. Laszczynski, B.L. Lucht, J. Electrochem. Soc. 167 (2020), 100519.
[14] K. Nie, Y. Hong, J. Qiu, Q. Li, X. Yu, H. Li, L. Chen, Front. Chem. 6 (2018) (616).
[15] K. Araki, N. Taguchi, H. Sakaebe, K. Tatsumi, Z. Ogumi, J. Power Sources 269 (2014) 236–243.
[16] M. Dong, Z. Wang, H. Li, H. Guo, X. Li, K. Shih, J. Wang, ACS Sustain. Chem. Eng. 5 (2017) 10199–10205.
[17] J.-Z. Kong, C. Ren, G.-A. Tai, X. Zhang, A.-D. Li, D. Wu, H. Li, F. Zhou, J. Power Sources 266 (2014) 433–439.
[18] G. Hu, M. Zhang, L. Wu, Z. Peng, K. Du, Y. Cao, ACS Appl. Mater. Interfaces 8 (2016) 33546–33552.
[19] M.R. Laskar, D.H. Jackson, S. Xu, R.J. Hamers, D. Morgan, T.F. Kuech, ACS Appl. Mater. Interfaces 9 (2017) 11231–11239.
[20] W. Cho, S.-M. Kim, J.H. Song, T. Yim, S.-G. Woo, K.-W. Lee, J.-S. Kim, Y.-J. Kim, J. Power Sources 282 (2015) 45–50.
[21] Y. Zhou, Y. Lee, H. Sun, J.M. Wallas, S.M. George, M. Xie, ACS Appl. Mater. Interfaces 9 (2017) 9614–9619.
[22] X. Xiong, Z. Wang, X. Yin, H. Guo, X. Li, Mater. Lett. 110 (2013) 4–9.
[23] S.J. Shi, J.P. Tu, Y.Y. Tang, Y.Q. Zhang, X.Y. Liu, X.L. Wang, C.D. Gu, J. Power Sources 225 (2013) 338–346.
[24] K. Min, K. Park, S.Y. Park, S.-W. Seo, B. Choi, E. Cho, J. Electrochem. Soc. 165 (2018) A79–A85.
[25] W. Cho, S.-M. Kim, K.-W. Lee, J.H. Song, Y.N. Jo, T. Yim, H. Kim, J.-S. Kim, Y.-J. Kim, Electrochim. Acta 198 (2016) 77–83.
[26] D.-J. Lee, B. Scrosati, Y.-K. Sun, J. Power Sources 196 (2011) 7742–7746.
[27] P. Yan, J. Zheng, J. Liu, B. Wang, X. Cheng, Y. Zhang, X. Sun, C. Wang, J.-G. Zhang, Nat. Energy 3 (2018) 600–605.
[28] C.-H. Jo, D.-H. Cho, H.-J. Noh, H. Yashiro, Y.-K. Sun, S.T. Myung, Nano Res. 8 (2014) 1464–1479.
[29] X.-D. Zhang, J.-L. Shi, J.-Y. Liang, L.-P. Wang, Y.-X. Yin, K.-C. Jiang, Y.-G. Guo, J. Power Sources 426 (2019) 242–249.
[30] Z. Chen, Y. Qin, K. Amine, Y.K. Sun, J. Mater. Chem. 20 (2010) 7606–7612.
[31] X. Xiong, D. Ding, Z. Wang, B. Huang, H. Guo, X. Li, J. Solid State Electrochem. 18 (2014) 2619–2624.
[32] Y. Ma, M. Xu, J. Zhang, R. Liu, Y. Wang, H. Xiao, Y. Huang, G. Yuan, J. Alloy. Compd. 848 (2020), 156387.
[33] Y. Cao, X. Qi, K. Hu, Y. Wang, Z. Gan, Y. Li, G. Hu, Z. Peng, K. Du, ACS Appl. Mater. Interfaces 10 (2018) 18270–18280.
[34] L. Song, F. Tang, Z. Xiao, Z. Cao, H. Zhu, A. Li, J. Electron. Mater. 47 (2018) 5896–5904.
[35] Q. Gan, N. Qin, Y. Zhu, Z. Huang, F. Zhang, S. Gu, J. Xie, K. Zhang, L. Lu, Z. Lu, ACS Appl. Mater. Interfaces 11 (2019) 12594–12604.
[36] G.-L. Xu, Q. Liu, K.K.S. Lau, Y. Liu, X. Liu, H. Gao, X. Zhou, M. Zhuang, Y. Ren, J. Li, M. Shao, M. Ouyang, F. Pan, Z. Chen, K. Amine, G. Chen, Nat. Energy 4 (2019) 484–494.
[37] T. Kim, L.K. Ono, Y. Qi, Adv. Mater. Interfaces 6 (2019) 12594–12604.
[38] S.H. Ju, I.S. Kang, Y.S. Lee, W.K. Shin, S. Kim, K. Shin, D.W. Kim, ACS Appl. Mater. Interfaces 6 (2014) 2546–2552.
[39] Y. Han, S. Heng, Y. Wang, Q. Qu, H. Zheng, ACS Energy Lett. 5 (2020) 2421–2433.
[40] J.-L. Shi, D.-D. Xiao, M. Ge, X. Yu, Y. Chu, X. Huang, X.-D. Zhang, Y.-X. Yin, X.-Q. Yang, Y.-G. Guo, L. Gu, L.-J. Wan, Adv. Mater. 30 (2018), 1705575.

[41] M. Frisch, G. Trucks, H. Schlegel, G. Scuseria, M. Robb, J. Cheeseman, G. Scalmani, V. Barone, B. Mennucci, G. Petersson, Gaussian09 (Revision D.01), I. Gaussian,, Wallingford, CT, 2013.
[42] R. Krishnan, J.S. Binkley, R. Seeger, J.A. Pople, J. Chem. Phys. 72 (1980) 650–654.
[43] S. Grimme, J. Antony, S. Ehrlich, H. Krieg, J. Chem. Phys. 132 (2010), 154104.
[44] T. Lu, F. Chen, J. Comput. Chem. 33 (2012) 580–592.
[45] Q. Zhou, J. Ma, S. Dong, X. Li, G. Cui, Adv. Mater. 31 (2019) (1902029).
[46] H. Xu, H. Zhang, J. Ma, G. Xu, T. Dong, J. Chen, G. Cui, ACS Energy Lett. 4 (2019) 2871–2886.
[47] A.M. Rocco, A. de Assis Carias, R.P. Pereira, Polymer 51 (2010) 5151–5164.
[48] G.I. Dzhardimalieva, I.E. Uflyand, J. Coord. Chem. 70 (2017) 1468–1527.
[49] Y.-G. Cho, S.-H. Jung, S.H. Joo, Y. Jeon, M. Kim, K.M. Lee, S. Kim, J.M. Park, H. K. Noh, Y.-S. Kim, J.-E. Hong, S.-I. Jeon, T. Kim, S.K. Kwak, H. Kong, H.-K. Song, J. Mater. Chem. A 6 (2018) 22483–22488.
[50] A. Banerjee, B. Ziv, Y. Shilina, S. Luski, I.C. Halalay, D. Aurbach, Adv. Energy Mater. 7 (2017), 1601556.
[51] R. Wang, J. Wang, S. Chen, Q. Yuan, D. Li, X. Zhang, L. Chen, Y. Su, G. Tan, F. Wu, Nano Energy 76 (2020), 105065.
[52] L.P. Wang, X.D. Zhang, T.S. Wang, Y.X. Yin, J.L. Shi, C.R. Wang, Y.G. Guo, Adv. Energy Mater. 8 (2018), 1801528.
[53] J.-H. Kim, S.J. Kim, T. Yuk, J. Kim, C.S. Yoon, Y.-K. Sun, ACS Energy Lett. 3 (2018) 3002–3007.
[54] E. Markevich, G. Salitra, Y. Talyosef, U.-H. Kim, H.-H. Ryu, Y.-K. Sun, D. Aurbach, A.C.S. Appl, Energy Mater. 1 (2018) 2600–2607.
[55] E. Markevich, G. Salitra, P. Hartmann, J. Kulisch, D. Aurbach, K.-J. Park, C.S. Yoon, Y.-K. Sun, J. Electrochem. Soc. 166 (2019) A5265–A5274.
[56] G.I. Dzhardimalieva, I.E. Uflyand, ChemistrySelect 3 (2018) 13234–13270.
[57] Y.-S. Kim, T.-H. Kim, H. Lee, H.-K. Song, Energy Environ. Sci. 4 (2011) 4038–4045.
[58] H. Li, A. Liu, N. Zhang, Y. Wang, S. Yin, H. Wu, J.R. Dahn, Chem. Mater. 31 (2019) 7574–7583.
[59] W. Huang, C.-Y. Wu, Y.-W. Zeng, C.-H. Jin, Z. Zhang, Acta Phys. Chim. Sin. 32 (2016) 2287–2292.
[60] M. Yoon, Y.-H. Dong, Y. Yoo, S. Myeong, J. Hwang, J. Kim, S.-H. Choi, J. Sung, S. J. Kang, J. Li, J. Cho, Adv. Funct. Mater. 30 (2019), 1907903.

Cheng Ma received the B.S. degree in 2014 and the M.S. degree in 2017 from Central South University, Changsha, China. He is pursuing his Ph.D. degree under the supervision of Prof. Weifeng Wei in State Key Laboratory of Powder Metallurgy, Central South University, Changsha, China. His current research focuses on functional electrolytes/separators and interfacial modification of electrodes for high-energy and safe batteries.

Minjian Chen is a graduate student in Powder Metallurgy Research Institute at Central South University, under the supervision of Prof. Weifeng Wei. His research focuses on the design and synthesis of solid polymer electrolyte and their applications for Lithium-ion batteries.

Dr. Zhengping Ding is now a lecturer in Changzhou University. He received his Bachelor's degree (2012) and Ph. D. degree in Materials Science (2017) from Central South University. Then, he worked as a R&D engineer at Tianjin Lishen Battery Joint-Stock Co., Ltd (2018), then he worked as a post-doctor in Electron Microscopy Laboratory at Peking University (2018–2020). He was awarded Jiangsu Provincial Double-Innovation Doctor in 2021. His main research interests focus on the synthesis and application of nanomaterials for clean energy storage, the relationship between structure and electrochemical properties and in-situ transmission electron microscopy in energy storage materials.

Bo Wei is currently pursuing his Ph.D. degree under the supervision of Prof. Ruifeng Zhang in the School of Materials Science and Engineering, Beihang University (China). His research interests include the study of the catalytic properties of transition metal carbonitride materials and the surface corrosion kinetics of metal materials by first principles calculation.

Dr. Chaoping Liang is currently an associate professor at central south university. He obtained his Ph.D. at central south university in 2013. From 2014–2017, he conducted Postdoc research with Prof. KJ Cho at University of Texas at Dallas. His research is committed to integrate computational and experimental materials research methods to design novel energy storage materials.

Dr. Liangjun Zhou is now Associate Professor in State Key Laboratory of Powder Metallurgy, Central South University. He obtained his B.S. from Huazhong University of Science and Technology in 2008 and got his Ph.D. from University of Chinese Academy of Sciences in 2014. His research interest mainly covers the design and synthesis of nanostructures and their application in nano-medicine, Li-S batteries and sodium/potassium ion batteries.

Dr. Libao Chen received his B.S. degree and M.S. degree from Central South University in 2001 and 2004 and Ph.D. degree from the Shanghai Institute of Microsystem and Information Technology, Chinese Academy of Sciences in 2007. He is now a professor in the State Key Laboratory of Power Metallurgy at Central South University. His main research interest is focused on the high-performance energy storage materials and devises, including Li alloy anode, Zinc anode, lithium ion batteries and lithium sulfur batteries.

Dr. Xiaobo Ji is a "Shenghua" Professor at Central South University and a Fellow of the Royal Society of Chemistry, specializing in the research and development of batteries and supercapacitor materials and their systems. He received his Ph. D. in Electrochemistry in 2007 under the supervision of Prof. Richard Compton at the University of Oxford and undertook postdoctoral work at MIT with Prof. Donald Sadoway.

Dr. Peng Gao is currently a Professor in School of Physics, Peking University, Beijing, China. He received his Ph.D. degree in 2010 from the Institute of Physics, Chinese Academy of Sciences. He was a post-doctoral fellow in University of Michigan (2010–2013), a research associate in Brookhaven National Laboratory (2013–2014), and a research fellow in University of Tokyo (2014–2015). He was selected in Project of Thousand Youth Talents and then joined in Peking University in 2015. His research interests include electron microscopy, ferroelectrics, solid-state ionics, and structure and properties of crystal defects and interfaces.

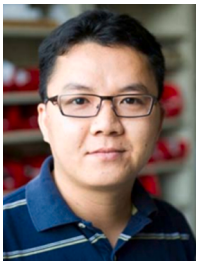

Dr. Weifeng Wei is a professor in the State Key Laboratory of Powder Metallurgy at the Central South University (China). After receiving his Ph.D. in Materials Engineering from the University of Alberta (2009), He joined the Sadoway Group as a postdoctoral research associate at MIT (2009–2011). His research concerns materials development in the fields of energy storage, including materials and device development for electrochemical supercapacitors and rechargeable batteries, and electrochemical recycling of spent materials in nonaqueous electrolytes.